Terahertz relaxation dynamics of a two-dimensional InSe multilayer

Wei Lu,[1,2] Zhibin Yang,[3,4] Jianhua Hao,[4] and Dong Sun[2,5,*]

[1]*State Key Laboratory of Precision Measurement Technology and Instruments, School of Precision Instruments and Opto-electronics Engineering, Tianjin University, No. 92 Weijin Road, Tianjin 300072, People's Republic of China*

[2]*International Center for Quantum Materials, School of Physics, Peking University, Beijing 100871, People's Republic of China*

[3]*Center for Terahertz Waves and College of Precision Instruments and Opto-electronics Engineering, Tianjin University, No. 92 Weijin Road, Tianjin 300072, People's Republic of China*

[4]*Department of Applied Physics, The Hong Kong Polytechnic University, Hung Hom, Hong Kong, People's Republic of China*

[5]*Collaborative Innovation Center of Quantum Matter, Beijing 100871, People's Republic of China*

(Received 25 March 2020; revised 2 July 2020; accepted 6 July 2020; published 29 July 2020)

Optical pump-terahertz probe measurements are performed to study the photoexcited carrier dynamics of the In-rich two-dimensional InSe multilayer, which is a promising candidate for future high performance electronic and photoelectronic applications. According to the transient terahertz measurements, the intraband and interband relaxation processes can be clearly identified from different carrier relaxation lifetimes. The intraband relaxation consists of an ultrafast (∼2 ps) carrier-optical phonon scattering and relatively slower (∼10 ps) anharmonic scattering of hot optical phonon. The subsequent interband recombination is dominated by a Shockley-Read-Hall recombination with lifetime on order of 100 ps. Because the grown polytype In-rich InSe multilayer has a high defect density, the primary recombination channel is through the defects in the surface, but the bulk recombination increases rapidly with temperature and can catch up the contribution of the surface recombination at high temperature.

DOI: 10.1103/PhysRevB.102.014314

I. INTRODUCTION

Indium selenide (InSe) is a traditional layered semiconducting material and atomically thin layers of InSe are rediscovered recently owing to its high mobility, quantum Hall effect, strong optical response, and other interesting properties [1–8]. The carrier mobility of InSe is comparable with black phosphorus (BP), a representative high mobility 2D semiconductor, while InSe has better chemical stability compared to BP [1]. InSe has a layer number dependent band gap which varies greatly from 1.26 eV to over 2.2 eV as the layer number decreases, inducing a broad spectral response [1–6]. Because of the large band gap and high mobility, InSe has large on/off ratio when used as channel material of transistors [1,5,7,8]. The band gap of InSe becomes direct as the number of layers is larger than 7 [2,5]. As a polar material, InSe also has relatively large In-Se polarization in intralayer, which results in a strong optical nonlinear effect that increases with thickness [9–12]. Therefore, InSe is a very promising material competitor for next generation electronic and optoelectronic applications.

Towards potential application in high performance electronic and photoelectronic devices based on InSe, it is critical to understand the dynamics of photoexcited carriers, which is the basic device physics that governs the optoelectronic and high-field response. Among the various ultrafast probes with different photon energies, a low-energy terahertz (THz) probe is sensitive to the intraband dynamics of photoexcited carriers that can determine the high-speed transport properties and the dynamics of (quasi)particles in a material [13,14]. Here, in this work, we use femtosecond visible/near-infrared pump and THz-probe transient spectroscopy to study the relaxation dynamics of photoexcited carriers of synthesized wafer-scale multilayer InSe. We found that the photoexcited carrier dynamics is insensitive to the photoexcitation intensity and pump photon energy, but strongly depends on the temperature. The initial intraband carrier relaxation is through carrier-optical phonon scattering (∼2 ps) and anharmonic phonon-phonon scattering (∼10 ps). Thereafter, Shockley-Read-Hall (SRH) recombination dominates the interband relaxation, which has typical decay lifetime of 100 ps, indicating the great influence of defect states on nonequilibrium carrier lifetime and radiative recombination. Our results provide necessary photoexcited carrier dynamics physics of InSe for its potential application for high performance electronic and optoelectronic devices.

II. EXPERIMENTAL DETAILS

The InSe thin films were prepared on sapphire substrates by pulsed laser deposition (PLD). The detailed information about the synthesis method and structural characteristics can be found in the previous work [6]. The energy dispersive x-ray spectrum (EDX) measurement shows the atomic ratio of In:Se ≈ 1.05:1. The structure characterization indicates that the obtained film is ε polytype of InSe. The thickness of the sample used in our measurement is $L = 10$ nm, which is approximately 12 layers taking an interlayer space of $d = 0.83$ nm. The film has a direct band gap of ∼1.37 eV based on the previous reports [6]. The transport measurement shows

*sundong@pku.edu.cn

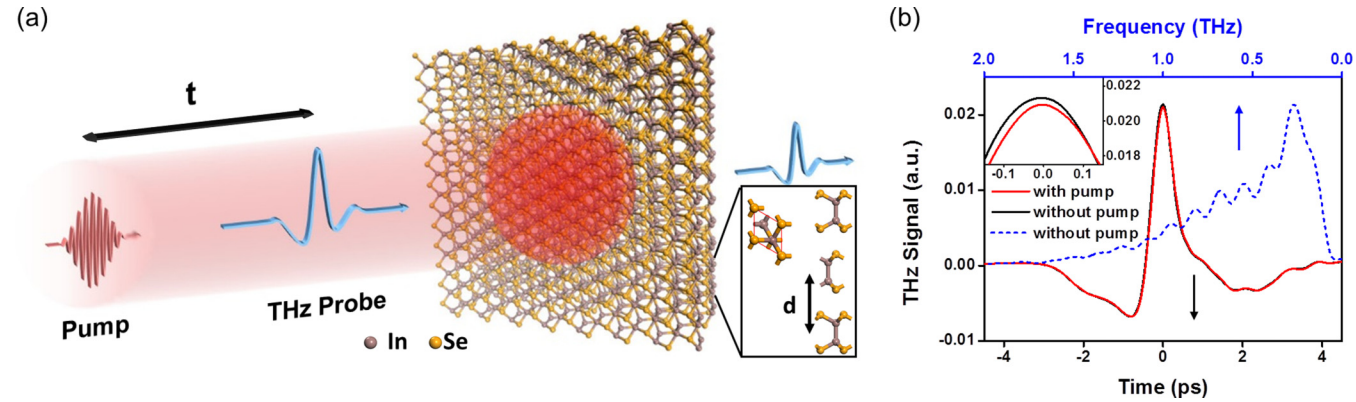

FIG. 1. (a) The schematic diagram of transient THz probe spectroscopic measurement and the lattice structure of ε-InSe. The inset is the unit-cell structure of InSe. (b) THz time-domain wave form transmitted through sample without (black line) and with (red line) pump excitation at zero delay time. The blue dash line is the frequency-domain terahertz wave form without pump excitation. The inset is the enlargement of THz peak in time domain.

that the sample is n type with an electron mobility $\mu = \sim 65\,\mathrm{cm}^2/\mathrm{V\,s}$ [6].

The experimental scheme of THz transmission and pump-probe spectroscopy measurements are the same as in our early work [15]. The InSe thin film is excited by either 1.53- or 3.06-eV 100-fs pump pulse, and the collinearly polarized THz probe pulse overlaps with the pump beam probe at various time delays as shown in Fig. 1(a). The spot sizes of pump and probe beams are ~1.2 and ~1.4 mm, respectively, ensuring a relative uniform photoexcited region for the THz probe. Since the photocarrier diffusion length is estimated to be on the order of 100 nm [6], which is far smaller than the beam sizes, the diffusion effect can be safely neglected with pump probe spot size over 1 mm. The pump-probe delay time t denotes the arrival time difference between the pump pulse and the THz pulse, and it is positive as the pump pulse arrived earlier to the sample.

III. RESULTS AND DISCUSSION

Figure 1(b) shows the typical transmission wave forms of THz in the time domain when the sample is unexcited (T_0) and excited (T) by the 1.53-eV pump at $t = 0$. From the inset, we can see the transmitted THz intensity slightly reduced ($\Delta T = T - T_0 < 0$) after the pump excitation because of the enhanced THz absorption by photocarriers (free carriers and excitons). Figure 2 shows the dynamical evolution of the transient THz response with different pump fluences at 78 K. The normalized response curves are overlapped with each other [Fig. 2(a)], indicating that the relaxation dynamics is independent of the photocarrier density ΔN in the pump fluence range. A similar phenomenon has also been observed in previous reports on mono/bilayer nanoflake and InSe single crystal [16,17]. The overall relaxation time of $\Delta T(t)$ from its peak to the noise background floor is ~800 ps. On the other hand, Fig. 2(b) shows the transient response at time zero, $\Delta T(0)$, increasing linearly with the pump fluence, which is consistent with the reported visible-band transient measurement of single crystal InSe [17].

The sample is n-doped with doping density (N_0) of $2 \times 10^{11}\,\mathrm{cm}^{-2}$, which is estimated from the mobility measurement with mobility $\mu = 65\,\mathrm{cm}^2\,\mathrm{V}^{-1}\,\mathrm{s}^{-1}$ at room temperature [6]. The absorption coefficient (α) for a 1.53-eV photon strongly depends on the crystal quality, layer number, doping density, strain, and so on; it falls into the range between 10^3 and $10^4\,\mathrm{cm}^{-1}$ according to the literature [17–21]. If we take

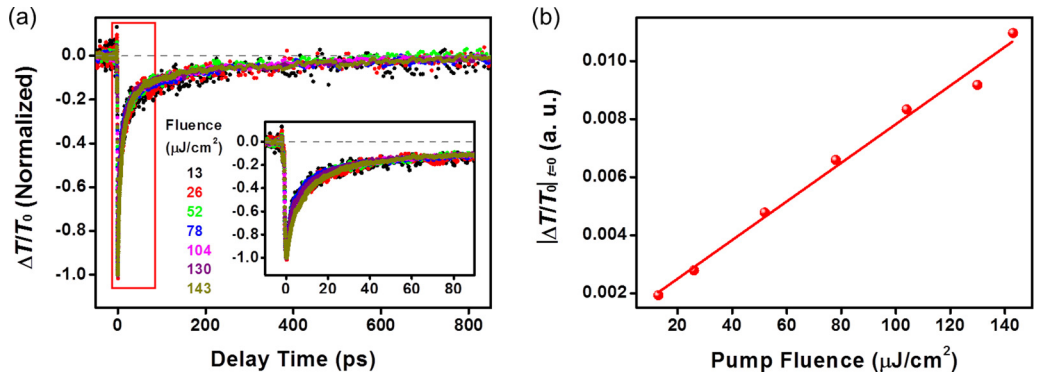

FIG. 2. Pump fluence dependence of transient THz dynamics of photoexcited carriers of InSe at 78 K. (a) Normalized transient transmission response of THz probe with 1.53-eV pump excitation. Inset is the enlargement of the part marked by the red box in the main plot. (b) $|\Delta T/T_0|_{t=0}$ as a function of pump fluence, whereas the solid line is the linear fit.

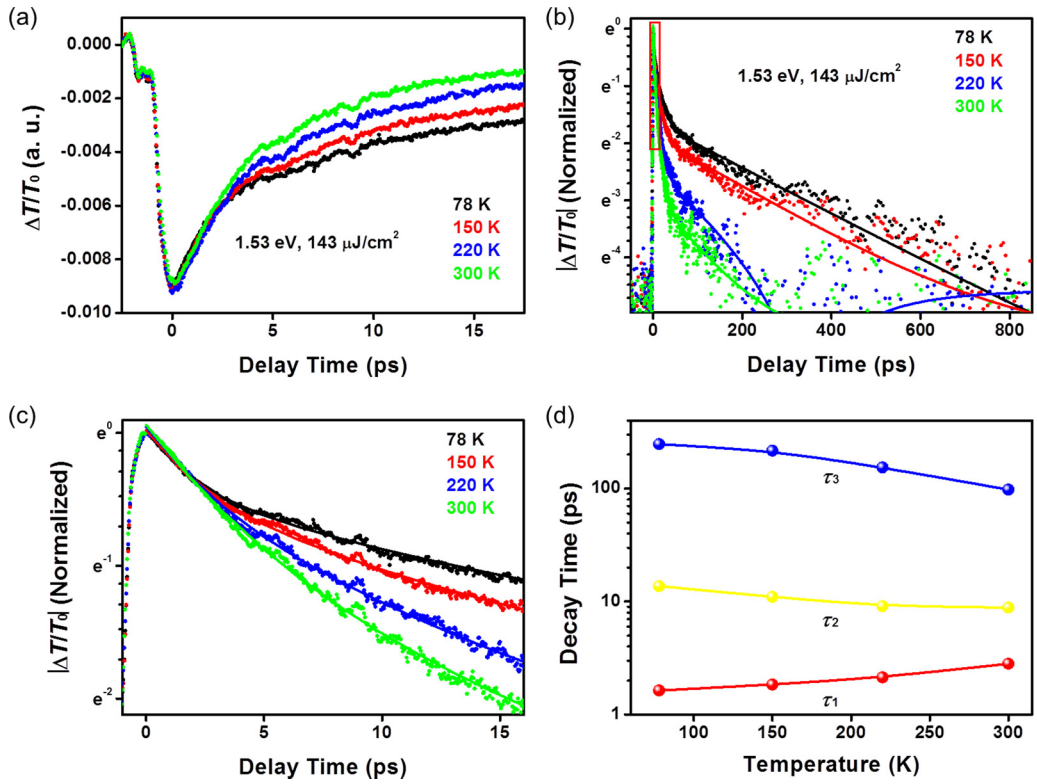

FIG. 3. Temperature dependence of transient THz dynamics of InSe excited with 1.53-eV pump. (a) Transient transmission response of THz probe at different temperatures with a pump fluence of 143 μJ/cm^2. (b) Semilog plots of normalized curves of (a), whereas the solid lines are fitting curves using Eq. (2). (c) Zoom-in plot of the two fast exponential decay components (as marked by red box) in (b), and (d) the temperature dependencies of the three decay time constants; the solid lines are guide to the eye.

$\alpha \sim 10^4$ cm^{-1} as a reasonable estimation [6], the photoexcited carrier density (ΔN) is estimated to range between 10^{12} and 10^{13} cm^{-2} taking a pump fluence range between 5.3×10^{13} and 5.8×10^{14} photon cm^{-2}, which is one to two orders larger than initial doping density before the excitation. Therefore, the overall carrier density N is dominated by ΔN, and then $N \approx \Delta N$. According to the pump power dependent measurement, the transient THz response has a linear relationship with excited carrier density ΔN [14]:

$$|\Delta T/T_0| \approx \sigma Z_0 L/(1+n) \approx \Delta N e \mu Z_0 L/(1+n), \quad (1)$$

under the approximation that $|\Delta T/T_0| \ll 1$ and $\omega\tau^* < 1$, where ω is the frequency of transmitted THz wave center at 0.3 THz in this work [Fig. 1(b)], and τ^* is carrier scattering time which is usually faster than 10^{-13} s [13,14], σ is the conductivity, $Z_0 = 377\ \Omega$ is the impedance of free space, $n \approx 3$ is the effective refractive index of InSe at THz frequencies [16], and e is the electron charge. Thereby, $|\Delta T/T_0|$ is proportional to $\Delta N\mu$. ΔN is directly proportional to the pump fluence when the excitation is below the saturation density [22–24].

Figure 3 shows the temperature dependence of photoexcited carrier dynamics with excitation pump fluence of 143μJ/cm^2. At different temperatures, $\Delta T(0)/T_0$ are almost the same [Fig. 3(a)] implying the initial transient signal immediately after the pump excitation is not sensitive to thermal vibration of lattice under the measured temperature range. As temperature increases from 78 to 300 K, the recovering time of the transient signal decreases from ~800 to ~300 ps. Furthermore, we notice that there are three clear decay components as can be fitted with logarithmic plot shown in Figs. 3(b) and 3(c). Thereby, we can fit the transient THz relaxation by triexponential function:

$$\Delta T/T_0 = A_0 + \sum A_i \times \exp(-t/\tau_i)\ \ (i = 1, 2, 3), \quad (2)$$

where A_i are the amplitude of exponential components and τ_i are the correspondent decay time constants. Here we note that our attempts to fit the transient dynamical curves at different temperatures with either a biexponential function [$A_0 + \sum A_i \times \exp(-t/\tau_i)(i = 1, 2)$], a power-law function (τ^{-a}), or a complex of monoexponential and power-law functions [$A_0 + A_1 \times \exp(-t/\tau) + A_2 \times t^{-a}$] all failed. Figure 3(d) shows the temperature dependencies of the exponential decay time constants τ_i as the temperature increases from 78 to 300 K: the fastest decay component τ_1 increases monotonically from 1.6 to 2.8 ps, while τ_2 and τ_3 decrease from ~13.7 to ~8.9 ps and from ~250 to 100 ps respectively.

To identify the three exponential decay components, which are the key to understanding the transient dynamics of InSe, transient measurements with higher pump photon energy (3.06 eV) are performed and the results are shown in Fig. 4. Compared to the 1.53-eV pump, which corresponds to transitions at the vicinity of the band edge, the 3.06-eV pump excites carriers to much higher initial carrier energy. The initial interaction of the photoexcited carriers with THz probe is mainly through intraband processes due to a relatively large energy gap of InSe (~1.37 eV). The very low photon

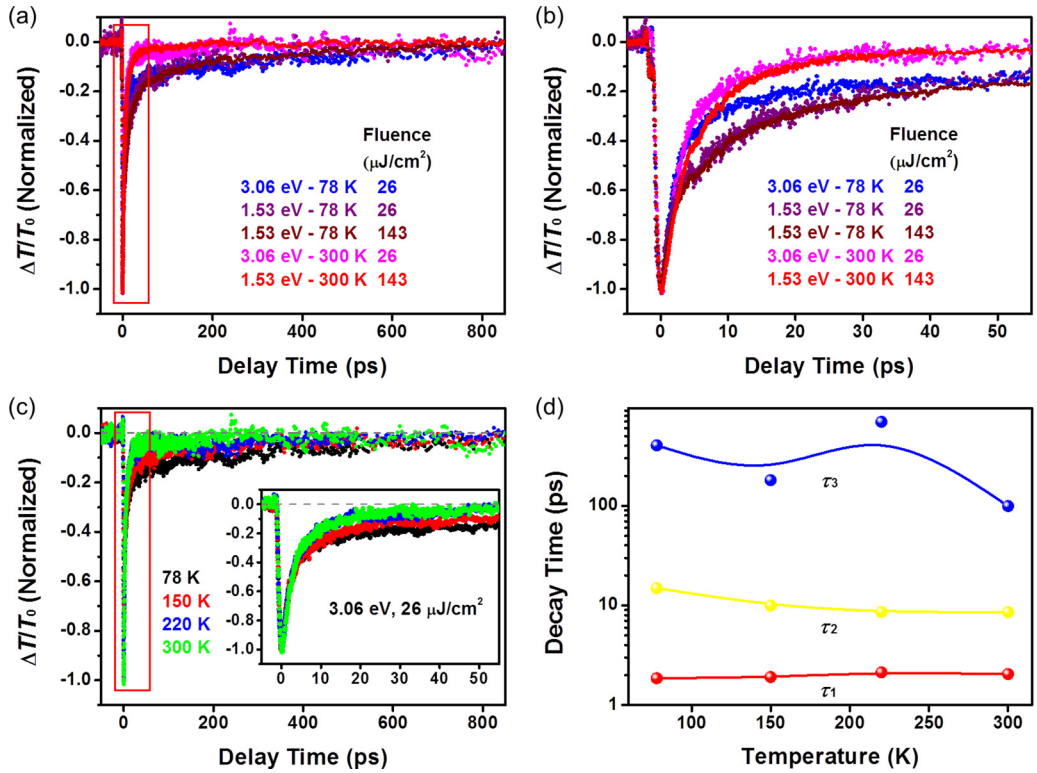

FIG. 4. (a) The comparison of the THz responses excited by 3.06- and 1.53-eV pumps, respectively. (b) The zoom-in plot of the red box part of (a). (c) The plot of normalized transient transmission response of THz probe at different temperatures with pump fluence of 26 μJ/cm^2 at 3.06 eV. Inset is the zoon-in plot of the red box part. (d)The temperature dependencies of decay time constants fitted by using triexponential function; the solid lines are guide to the eye.

energy of the THz probe (1 THz–4.1 meV) is sensitive to the changes of photoexcited carriers distributions, and the intraband relaxation process to the band edge of photoexcited carriers after the excitation of 3.06 eV is more rapid than that of the 1.53-eV excitation.

Figures 4(a) and 4(b) compare the transient dynamics for the 3.06- and 1.53-eV excitation at both room temperature and 78 K. The initial relaxation (the first tens of ps) is clearly faster for the 3.06-eV pump, and this difference is more prominent at lower temperature [Fig. 4(b)]. However, after the initial relaxation, the normalized relaxation curves become very similar thereafter [Fig. 4(a)]. Figure 4(c) shows the temperature dependence of transient dynamics excited with the 3.06-eV pump. The two fast decay time constants (τ_1 and τ_2) both have clear temperature dependence as shown in Fig. 4(d): τ_1 increases monotonically as temperature increases and τ_2 decreases monotonically as temperature increases, while τ_3 doesn't show clear temperature dependence. The temperature dependence of $\tau_{1/2}$ indicates that higher pump energy can significantly modify the fast decay process(es) which corresponds to the intraband relaxation. The temperature dependence of $\tau_{1/2}$ is similar between 3.06- and 1.53-eV pump excitation [Figs. 3(d) and 4(d)]. τ_3 shows a large variation and no clear tendency with temperature, mainly because of the large experimental error, which arises from the lower signal-to-noise ratio at the decay tails at long delay time, so the fitting results of τ_3 has large uncertainties and its temperature dependence shown in Fig. 4(d) is not conclusive.

According to the temperature and pump-photon energy dependent results, we can attribute different decay time constants to different photoexcited carrier relaxation processes. The initial transient relaxation dynamics relating to τ_1 and τ_2 are both attributed to intraband relaxation of carriers. After the pump excitation and the initial rapid carrier-carrier scattering processes ($< \sim$100 fs, within the excitation pulse width), the photoexcited electron/hole reaches a thermal equilibrium. Thereafter, the relaxation of hot carriers is initially dominated by large energy optical phonon scattering, which accounts for the decay time constant τ_1, on the order of a few ps depending on the temperature. This decay time constant ($\sim$2 ps) is consistent with the hot carrier cooling time (1–3.5 ps) of bulk InSe measured by visible light [17], but shorter than that of mono/bilayer InSe nanoflake ($\sim$4 ps) [16]. The differences are possibly due to the difference in electronic structure, exciton states with large binding energy in mono/bilayer InSe [1,3], and the chemical modification on the nanoflake.

Once the carrier temperatures cool down to reach an equilibrium with the hot optical phonons, further intraband relaxation of carriers relies on the cooling of hot optical phonons through the anharmonic phonon-phonon scattering effect [15,22] to couple to low-energy acoustic phonons. These processes, which account for the time constant τ_2 observed in our measurements, persist until the photoexcited carriers relax to the band edge and reach thermal equilibrium with the lattice. The measured total intraband relaxation time, which is composed of τ_1 and τ_2, is consistent with transient absorption measurement result (12–16 ps) of InSe

nanoparticles [25]. τ_2 is also consistent with the previously reported typical phonon lifetime of 10 ps [22,26]. The optical phonon lifetime of InSe is longer than many conventional semiconductors [26–28], such as GaAs, GaN, ZnSe, due to the presence of large phononic band gaps and low group velocities of optical phonons [17,29]. Here we note Auger recombination and certain multiexciton recombination processes can possibly match the time scales of τ_1 and τ_2. However, Auger recombination, multiexciton recombination [30–33], and exciton-exciton annihilation [34,35] all should have nonlinearly pump power dependence, which doesn't match the power dependencies shown in Fig. 2. On the other hand, the Auger recombination rate is extremely small for wide-band semiconductors [26]. The multiexciton population can also be safely ignored at the measurement temperature [32], because the multiexciton binding energy is only a fraction of free exciton binding energy (∼14.5 meV for bulk InSe [36,37]) [38–40].

The above intraband relaxation process can be further described by a set of rate equations based on the extended two-temperature model [15]:

$$\begin{aligned}\frac{dT_e}{dt} &= -\beta\frac{T_e - T_{op}}{\tau_1},\\ \frac{dT_{op}}{dt} &= \beta\frac{C_e}{C_{op}}\frac{T_e - T_{op}}{\tau_1} - \gamma\frac{T_{op} - T_L}{\tau_2},\end{aligned} \tag{3}$$

where T_e is the quasiequilibrium temperature of photoexcited electron/holes, T_{op} is the temperature of coupled optical phonons, T_L is the temperature of lattice, β and γ are the coefficients that describe the electron-optical phonon coupling and arharmonic phonon-phonon coupling strength, C_e and C_{op} are the specific heat of electron and optical phonon, respectively. Here the instantaneous energy transfer process from photon to electron during the pump excitation is ignored, which is much shorter than the experimental time resolution. The model also doesn't include the nonradiative recombination process which should be minor during the rapid intraband relaxation period due to the larger band gap and long carrier recombination time. The temperature dependence of τ_1 observed in Fig. 3(d) (with 1.53-eV excitation) and Fig. 4(d) (with 3.06-eV excitation) indicates that the electron-optical phonon coupling β gets weaker when the temperature increases. This is explained by the fact that the phonon density and subsequent phonon reabsorption by carriers are enhanced at higher temperature, leading to a slower optical phonon scattering strength [larger τ_1, Figs. 3(d) and 4(b)] [41]. On the other hand, the temperature dependence of τ_2 indicates the anharmonic phonon-phonon scattering strength γ gets stronger when the temperature increases [26–28,42–44].

After the initial intraband relaxation processes, we attribute the further relaxation dynamics observed in our experiment to interband recombination. The InSe is polycrystalline film with high density of defect states (atomic ratio of In:Se = 1.05:1) [6], especially on the surfaces, which can act as trapping centers [45]. Given that the photoexcited carrier density (10^{12}–10^{13} cm^{-2}) is far larger than the doping density (∼2 × 10^{11} cm^{-2}), if this recombination process is dominated by radiative recombination of photoexcited carriers, the recombination time should show a carrier density dependence, which contradicts the observation in the pump power dependent measurement [Fig. 2(a)]. So we attribute τ_3 to the trap assisted recombination (i.e., SRH effect). Therefore, the effective carrier recombination lifetime τ_{SRH} can be formulated as [46]

$$(\tau_{SRH})^{-1} = (\tau_b)^{-1} + 2[L/2S + (L/\pi)^2 D^{-1}]^{-1}. \tag{4}$$

The equation consists of two terms: the first term accounts for the recombination in the bulk, where τ_b is the bulk carrier recombination lifetime; the second term on the right-hand side accounts for the surface recombination. The surface recombination term consists of two parts: the first half ($L/2S$), accounts for the out-of-plane surface recombination, where $L \sim 10$ nm is the thickness of the InSe flake, S is the surface recombination velocity; the second half $[(L/\pi)^2 D^{-1}]$ accounts for the diffusion to the surface, where $D = \mu k_B T_L/e$ is the ambipolar diffusion coefficient. The $(L/\pi)^2 D^{-1}$ term is estimated to be on the order of 10^{-12} s; since $\tau_3 \sim \tau_{SRH}$ is on order of 10^{-10} s as measured in our experiment, the contribution of the diffusion term $[(L/\pi)^2 D^{-1}]$ is negligible. Furthermore, since the sample thickness of 10 nm is far smaller than its micrometer scale penetration depths according to the absorption coefficients of 10^3–10^4 cm^{-1} of our pump beams [17–21], the carrier density is approximately homogeneous along the out-of-plane direction. Therefore, the influence of carrier diffusion along the out-of-plane direction can be neglected, and the surface recombination dynamics is independent of the photoexcitation energy.

For the bulk recombination term, the recombination time τ_b follows the following SRH recombination rate [47–49]:

$$(\tau_b)^{-1} = N_t v \sigma_n \sigma_p (N_0 + P_0 + \Delta N)/[\sigma_n (N_0 + \Delta N + N_1) + \sigma_p (P_0 + \Delta P + P_1)], \tag{5}$$

where N_t is the trapping state density in bulk, $v = (3k_B T_L/m^*)^{1/2}$ is carrier thermal velocity, m^* is the carrier effective mass, $\sigma_{n(p)}$ is the capture cross section of electron (hole), P_0 is the equilibrium hole density, ΔP is the photoexcited hole density, $N_1 = N_c \exp[(E_t - E_c)/k_B T_L]$, $P_1 = N_v \exp[-(E_t - E_v)/k_B T_L]$, $N_{c(v)}$, is the effective density of state at the conduction (valence) band, E_t is the trapping level energy, and $E_{c(v)}$ is the conduction (valence)-band edge energy. Because an efficient trapping level lies in the band gap of a wide-band-gap semiconductor, both N_1 and P_1 are very small when the thermal energy is much smaller than the band gap. After the photoexcitation, because the photoexcited carrier density is much higher than intrinsic doping level, $\Delta N \approx \Delta P \gg N_0$, P_0, N_1, and P_1. Making an approximation $\sigma_p \propto \sigma_n$ [48], the bulk recombination rate follows $(\tau_b)^{-1} \propto N_t v \sigma_n$, which has very similar form with the recombination at the surfaces: $S \propto N_s v \sigma_s$, with the trapping state density and capture cross section replaced with N_s and σ_s. According

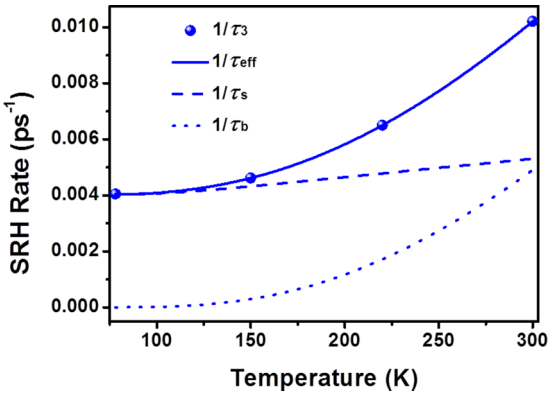

FIG. 5. The fitting of temperature dependence of carrier recombination rate for 1.53-eV excitation with Eq. (6). The solid line is the fitting curve, and the dash and dot lines are contributions from surface and bulk, respectively.

to $\sigma_n = \sigma_\infty \exp(-E_a/k_B T_L)$, where E_a is capture activation energy of trapping center, equivalent to value of trap depth subtracted from emission activation energy [50], therefore, Eq. (4) can be rewritten as

$$\begin{aligned}(\tau_{\text{eff}})^{-1} &= C_t N_t \upsilon \sigma_n + C_s N_s \upsilon \sigma_s \\ &= (k_B T_L)^{1/2}[C_1 \exp(-E_a/k_B T_L) \\ &\quad + C_2 \exp(-E_{\text{sa}}/k_B T_L)],\end{aligned} \tag{6}$$

where C_i $(i = 1, 2, t, s)$ is constant, and E_{sa} is the capture activation energy of trapping center on the surface.

The fitting of the temperature dependence of τ_3 with Eq. (6) is shown in Fig. 5, indicating the SRH recombination is the mechanism behind the slow process. The surface recombination has very weak temperature dependence and it dominates the recombination at the low temperature. On the contrary, τ_b increases rapidly as temperature increases, and catches up the contribution of surface recombination at room temperature. This indicates that the recombination through the defect states has different activation energy and the capture of carrier in the bulk more relies on the phonon scattering process. The SRH recombination lifetime determined by in this work has the same order of magnitude with the transient photoluminescence and reflection measurement results on InSe single crystal and nanoparticle samples by Zhong and Yang [17,25] although our sample may have higher defect density.

In summary, our optical pump-THz probe measurements on 2D In-rich InSe multilayer show that the carrier dynamics is not sensitive to excitation density and photon energy, but strongly depends on temperature. The initial rapid cooling of photocarriers relies on the carrier optical phonon scattering with characteristic decay time constant of ~2 ps. The cooling thereafter is dominated by the hot optical phonon emission with characteristic time constant of ~10 ps, which decreases with temperature because of the enhancement of anharmonic phonon scattering. The slow carrier recombination process is mainly through the defect states and the SHR effect dominates the recombination with a lifetime on a scale of 100 ps. Our simulation shows the recombination on surfaces is more efficient than that in bulk at low temperature, but the bulk recombination increases rapidly as temperature increases and becomes equally important with surface recombination at room temperature. Our results provide necessary photoexcited carrier dynamics for potential future high performance electronic and photoelectronic applications based on InSe.

ACKNOWLEDGMENTS

This project has been supported by the National Natural Science Foundation of China (NSFC Grants No. 11704012, No. 11674013, and No. 91750109), the Recruitment Program of Global Experts, and the Research Grants Council (RGC) of Hong Kong (RGC GRF No. PolyU 153023/18P).

[1] D. A. Bandurin, A. V. Tyurnina, G. L. Yu, A. Mishchenko, V. Zólyomi, S. V. Morozov, R. K. Kumar, R. V. Gorbachev, Z. R. Kudrynskyi, S. Pezzini, Z. D. Kovalyuk, U. Zeitler, K. S. Novoselov, A. Patanè, L. Eaves, I. V. Grigorieva, V. I. Fal'ko, A. K. Geim, and Y. Cao, High electron mobility, quantum Hall effect and anomalous optical response in atomically thin InSe, Nat. Nanotechnol. **12**, 223 (2016).

[2] G. W. Mudd, S. A. Svatek, T. Ren, A. Patanè, O. Makarovsky, L. Eaves, P. H. Beton, Z. D. Kovalyuk, G. V. Lashkarev, Z. R. Kudrynskyi, and A. I. Dmitriev, Tuning the bandgap of exfoliated InSe nanosheets by quantum confinement, Adv. Mater. **25**, 5714 (2013).

[3] J. F. Sánchez-Royo, G. Muñoz-Matutano, M. Brotons-Gisbert, J. P. Martínez-Pastor, A. Segura, A. Cantarero, R. Mata, J. Canet-Ferrer, G. Tobias, E. Canadell, J. Marqués-Hueso, and B. D. Gerardot, Electronic structure, optical properties, and lattice dynamics in atomically thin indium selenide flakes, Nano Res. **7**, 1556 (2014).

[4] Z. Chen, J. Biscaras, and A. Shukla, A high performance graphene/few-layer InSe photo-detector, Nanoscale **7**, 5981 (2015).

[5] M. Osman, Y. Huang, W. Feng, G. Liu, Y. Qiu, and P. Hu, Modulation of opto-electronic properties of InSe thin layers via phase transformation. RSC Adv. **6**, 70452 (2016).

[6] Z. Yang, W. Jie, C.-H. Mak, S. Lin, H. Lin, X. Yang, F. Yan, S. P. Lau, and J. Hao, Wafer-Scale synthesis of high-quality semiconducting two-dimensional layered InSe with broadband photoresponse, ACS Nano **11**, 4225 (2017).

[7] W. Feng, W. Zheng, W. Cao, and P. Hu, Back gated multilayer InSe transistors with enhanced carrier mobilities via the suppression of carrier scattering from a dielectric interface, Adv. Mater. **26**, 6587 (2014).

[8] S. Sucharitakul, N. J. Goble, U. R. Kumar, R. Sankar, Z. A. Bogorad, F.-C. Chou, Y.-T. Chen, and X. P. A. Gao, Intrinsic electron mobility exceeding $10^3 \text{cm}^2/(\text{V s})$ in multilayer InSe FETs, Nano Lett. **15**, 3815 (2015).

[9] I. M. Catalano, A. Cingolani, C. Calí, and S. Riva-Sanseverino, Second harmonic generation in InSe, Solid State Commun. **30**, 585 (1979).

[10] A. Bourdon, E. Bringuier, M. T. Portella, M. Vivières, and N. Piccioli, Angular Properties of Second-Harmonic Polarization

Due to High-Order Nonlinearities: Application to GaSe and InSe, Phys. Rev. Lett. **65**, 1925 (1990).

[11] E. Bringuier, A. Bourdon, N. Piccioli, and A. Chevy, Optical second-harmonic generation in lossy media: Application to GaSe and InSe, Phys. Rev. B **49**, 16971 (1994).

[12] Q. Hao, H. Yi, H. Su, B. Wei, Z. Wang, Z. Lao, Y. Chai, Z. Wang, C. Jin, J. Dai, and W. Zhang, Phase identification and strong second harmonic generation in pure ε-InSe and Its alloys, Nano Lett. **19**, 2634 (2019).

[13] R. Ulbricht, E. Hendry, J. Shan, T. F. Heinz, and M. Bonn, Carrier dynamics in semiconductors studied with time-resolved terahertz spectroscopy, Rev. Mod. Phys. **83**, 543 (2011).

[14] F. A. Hegmann, O. Ostroverkhova, and D. G. Cooke, Probing organic semiconductors with terahertz pulses, in *Photophysics of Molecular Materials*, edited by G. Lanzani (WileyVCH Verlag GmbH & Co. KGaA, 2005), p. 367.

[15] W. Lu, J. Ling, F. Xiu, and D. Sun, Terahertz probe of photoexcited carrier dynamics in the Dirac semimetal Cd_3As_2, Phys. Rev. B **98**, 104310 (2018).

[16] J. Lauth, A. Kulkarni, F. C. M. Spoor, N. Renaud, F. C. Grozema, A. J. Houtepen, J. M. Schins, S. Kinge, and L. D. A. Siebbeles, Photogeneration and Mobility of Charge Carriers in Atomically Thin Colloidal InSe Nanosheets Probed by Ultrafast Terahertz Spectroscopy, J. Phys. Chem. Lett. **7**, 4191 (2016).

[17] C. Zhong, V. K. Sangwan, J. Kang, J. Luxa, Z. Sofer, M. C. Hersam, and E. A. Weiss, Hot carrier and surface recombination dynamics in layered InSe crystals, J. Phys. Chem. Lett. **10**, 493 (2019).

[18] R. W. Damon and R. W. Redington, Electrical and optical properties of indium selenide, Phys. Rev. **96**, 1498 (1954).

[19] M. M. El-Nahass, A.-B. A. Saleh, A. A. A. Darwish, and M. H. Bahlol, Optical properties of nanostructured InSe thin films, Opt. Commun. **285**, 1221 (2012).

[20] A. R. Goi, A. Cantarero, U. Schwarz, K. Syassen, and A. Chevy, Low-temperature exciton absorption in InSe under pressure, Phys. Rev. B **45**, 4221 (1992).

[21] F. J. Manjón, D. Errandonea, A. Segura, V. Muñoz, G. Tobías, P. Ordejón, and E. Canadell, Experimental and theoretical study of band structure of InSe and $In_{1-x}Ga_xSe$ ($x < 0.2$) under high pressure: Direct to indirect crossovers, Phys. Rev. B **63**, 125330 (2001).

[22] M. Fox, *Optical Properties of Solids*, 2nd ed. (Oxford University Press, New York, 2011).

[23] P. C. Becker, D. Lee, A. M. Johnson, A. G. Prosser, R. D. Feldman, R. F. Austin, and R. E. Behringer, Femtosecond Dynamics of Resonantly Excited Room-Temperature Excitons in II-VI CdZnTe/ZnTe Quantum Wells, Phys. Rev. Lett. **68**, 1876 (1992).

[24] S. Schmitt-Rink, D. S. Chemla, and D. A. B. Miller, Theory of transient excitonic optical nonlinearities in semiconductor quantum-well structures, Phys. Rev. B **32**, 6601 (1985).

[25] S. Yang and D. F. Kelley, Transient absorption spectra and dynamics of InSe nanoparticles, J. Phys. Chem. B **110**, 13430 (2006).

[26] B. K. Ridley, *Quantum Processes in Semiconductors*, 5th ed. (Oxford University Press, New York, 2013).

[27] T. Beechem and S. Graham, Temperature and doping dependence of phonon lifetimes and decay pathways in GaN, J. Appl. Phys. **103**, 093507 (2008).

[28] S. Anand, P. Verma, K. P. Jain, and S. C. Abbi, Temperature dependence of optical phonon lifetimes in ZnSe, Phys. B: Condens. Matter **226**, 331 (1996).

[29] H. Zhou, Y. Cai, G. Zhang, and Y.-W. Zhang, Unusual phonon behavior and ultra-low thermal conductance of monolayer InSe, Nanoscale **10**, 480 (2018).

[30] V. I. Klimov, Mechanisms for photogeneration and recombination of multiexcitons in semiconductor nanocrystals: implications for lasing and solar energy conversion, J. Phys. Chem. B **110**, 16827 (2006).

[31] V. I. Klimov, J. A. McGuire, R. D. Schaller, and V. I. Rupasov, Scaling of multiexciton lifetimes in semiconductor nanocrystals, Phys. Rev. B **77**, 195324 (2008).

[32] Y. You, X.-X. Zhang, T. C. Berkelbach, M. S. Hybertsen, D. R. Reichman, and T. F. Heinz, Observation of biexcitons in monolayer WSe2, Nat. Phys. **11**, 477 (2015).

[33] N. S. Makarov, S. Guo, O. Isaienko, W. Liu, I. Robel, and V. I. Klimov, Spectral and dynamical properties of single excitons, biexcitons, and trions in Cesium–Lead-Halide perovskite quantum dots, Nano Lett. **16**, 2349 (2016).

[34] Y.-Z. Ma, L. Valkunas, S. L. Dexheimer, S. M. Bachilo, and G. R. Fleming, Femtosecond Spectroscopy of Optical Excitations in Single-Walled Carbon Nanotubes: Evidence for Exciton-Exciton Annihilation, Phys. Rev. Lett. **94**, 157402 (2005).

[35] N. Kumar, Q. Cui, F. Ceballos, D. He, Y. Wang, and H. Zhao, Exciton-exciton annihilation in $MoSe_2$ monolayers, Phys. Rev. B **89**, 125427 (2014).

[36] J. Camassel, P. Merle, H. Mathieu, and A. Chevy, Excitonic absorption edge of indium selenide, Phys. Rev. B **17**, 4718 (1978).

[37] P. Dey, J. Paul, N. Glikin, Z. D. Kovalyuk, Z. R. Kudrynskyi, A. H. Romero, and D. Karaiskaj, Mechanism of excitonic dephasing in layered InSe crystals, Phys. Rev. B **89**, 125128 (2014).

[38] J. Singh, D. Birkedal, V. G. Lyssenko, and J. M. Hvam, Binding energy of two-dimensional biexcitons, Phys. Rev. B **53**, 15909 (1996).

[39] D. A. Kleinman, Binding energy of biexcitons and bound excitons in quantum wells, Phys. Rev. B **28**, 871 (1983).

[40] D. Birkedal, J. Singh, V. G. Lyssenko, J. Erland, and J. M. Hvam, Binding of Quasi-Two-Dimensional Biexcitons, Phys. Rev. Lett. **76**, 672 (1996).

[41] Y. Yang, D. P. Ostrowski, R. M. France, K. Zhu, J. van de Lagemaat, J. M. Luther, and M. C. Beard, Observation of a hot-phonon bottleneck in lead-iodide perovskites, Nat. Photon. **10**, 53 (2015).

[42] A. Debernardi, S. Baroni, and E. Molinari, Anharmonic Phonon Lifetimes in Semiconductors from Density-Functional Perturbation Theory, Phys. Rev. Lett. **75**, 1819 (1995).

[43] P. G. Klemens, Anharmonic decay of optical phonons, Phys. Rev. **148**, 845 (1966).

[44] K. H. Michel, S. Costamagna, and F. M. Peeters, Theory of anharmonic phonons in two-dimensional crystals, Phys. Rev. B **91**, 134302 (2015).

[45] K. Iordanidou, M. Houssa, J. Kioseoglou, V. V. Afanas'ev, A. Stesmans, and C. Persson, Hole-Doped 2D InSe for spintronic applications, ACS Appl. Nano Mater. **1**, 6656 (2018).

[46] A. B. Sproul, Dimensionless solution of the equation describing the effect of surface recombination on carrier decay in semiconductors, J. Appl. Phys. **76**, 2851 (1994).

[47] A. Schenk, A model for the field and temperature dependence of Shockley-Read-Hall lifetimes in silicon, Solid-State Electron. **35**, 1585 (1992).

[48] D. Macdonald and A. Cuevas, Validity of simplified Shockley-Read-Hall statistics for modeling carrier lifetimes in crystalline silicon, Phys. Rev. B **67**, 075203 (2003).

[49] E. Quiniou, O. Palais, D. Barakel, and I. Périchaud, Temperature dependent lifetime spectroscopy (TDLS) for the identification of metallic impurities, Energy Procedia **92**, 180 (2016).

[50] C. H. Henry and D. V. Lang, Nonradiative capture and recombination by multiphonon emission in GaAs and GaP, Phys. Rev. B **15**, 989 (1977).